Supplemental Figure Legends:

Supplemental Figure 1. αvβ8 integrin is expressed in perivascular tumor cells in human GBM samples. (A-D); Images of anti-β8 integrin immunohistochemistry stains of formalin-fixed and paraffin-embedded human non-cancerous human brain (A) and GBM sections (B-D). Note that β8 integrin protein is enriched in perivascular tumor cells. **(E);** Immunoblot analysis of β8 integrin protein levels in a non-cancerous brain sample (n=1) and in 11 different grade IV GBM lysates. Note that in comparison to the non-cancerous brain lysate, β8 integrin protein levels are higher in most GBM samples.

Supplemental Figure 2. Fractionation of primary GBM cells based on differential expression of β8 integrin protein. (A); Summary of percentages of cells expressing β8 integrin protein ($\beta8^{high}$ GBM cells) from 25 different freshly resected human tumor samples. **(B);** Representative FACS plots of $\beta8^{high}$ and $\beta8^{low}$ GBM cells from select freshly resected tumor samples listed in (A).

Supplemental Figure 3. Antibody-mediated inhibition of β8 integrin blocks GSC self-renewal and spheroid formation. (A, B); $\beta8^{high}$ GBM cells were treated with matching pre-immune rabbit serum (A) or antiserum directed against the β8 integrin extracellular domain (B). Note that the anti-β8 integrin antibody treatment diminishes GBM cell growth and sphere formation. **(C);** Quantitation of sphere size after four days in culture with control serum or the anti-β8 integrin neutralizing antiserum (1:50 dilution). Spheres formed in the presence of the anti-β8 integrin are consistently smaller. **(D);** Analysis of ITGB8 mRNA expression levels in

primary human GBM cells before (CSC) and after (FCS) serum-mediated differentiation based on transcriptome sequencing of single cells (top row) and tumorigenic potential in vivo (bottom row). These data were mined from Patel et al. (2014), *Science* 344: 1396-1401.

Supplemental Figure 4. β8 integrin in primary GSCs promotes tumor initiation and growth in vivo. (A); Representative FACS plot of $\beta8^{high}$ and $\beta8^{low}$ tumor cells from a freshly resected GBM sample (HBT28). **(B, C);** H&E stained and immunofluorescence images of brain sections from mice injected with $\beta8^{high}$ GBM cells sorted from sample HBT28. Note that $\beta8^{high}$ cells form large intracranial tumors with cancer cells displaying invasion along white matter and blood vessels. **(D, E);** H&E and immunofluorescence images of tumor sections from mice injected with $\beta8^{low}$ GBM cells fractionated from HBT28 samples. **(F);** Representative FACS plot of $\beta8^{high}$ and $\beta8^{low}$ tumor cells from freshly resected GBM sample HBT38. **(G, H);** H&E stained and immunofluorescence images of brain sections from mice injected with $\beta8^{high}$ GBM cells sorted from sample HBT38. Note that $\beta8^{high}$ cells form diffuse and invasive intracranial tumors. **(I, J);** H&E stained and immunofluorescence images from mouse brains injected with $\beta8^{low}$ GBM cells sorted from sample HBT38.

Supplemental Figure 5. Immunofluorescence analysis of xenograft tumors derived from $\beta8^{high}$ GBM cells. (A-F); Double immunofluorescence stains of β8 integrin-dependent GBM growth, invasion and angiogenesis in xenograft tumors (HBT28). $\beta8^{high}$ cells express vimentin and nestin and generate well-vascularized and invasive tumors that are interlaced with glial cells as revealed by anti-laminin stains for vascular basement membranes (A, B) anti-GFAP for astrocytes (C, D), and anti-IBA1 for microglia (E, F) double labeling.

Supplemental Figure 6. Analysis of β8 integrin re-expression in $\beta8^{low}$ GSCs. (A); An H&E-stained coronal section through a mouse brain harboring a tumor derived from unfractionated cells from human sample HBT32. **(B);** FACS-based fractionation of $\beta8^{high}$ and $\beta8^{low}$ human cells from HBT32 xenograft. A human-specific CD47 antibody was used in combination with anti-β8 integrin to distinguish human and mouse cells. **(C, D);** $\beta8^{high}$ (C) and $\beta8^{low}$ (D) GBM cells fractionated from the xenograft tumor in panel A generate secondary tumors in mice. **(E-H);** Anti-β8 integrin immunohistochemistry reveals integrin expression in intracranial tumors derived from both $\beta8^{high}$ (E, G) and $\beta8^{low}$ (F, H) GBM cells. Panels G and H are higher magnification images of boxed areas in panels E and F. Scale bars in C-F are 50 μm and G, H are 20 μm. **(I);** FACS-based fractionation of $\beta8^{high}$ and $\beta8^{low}$ GBM cells from the HBT14 xenograft. **(J, K);** Both $\beta8^{high}$ GBM (J) and $\beta8^{low}$ GBM cells (K) that form spheroids in culture show robust integrin expression, as determined by FACS.

Supplemental Figure 7. Cerebral blood vessel co-option in xenograft tumors. (A); GFP-expressing $\beta8^{WT}$ GSCs were intracranially implanted into the mouse brain. One month later sections were immunofluorescently labeled with anti-GFP and anti-CD31 antibodies, revealing juxtaposition between tumor cells and cerebral blood vessels. **(B);** TGFβ1 ELISA from freshly sorted $\beta8^{high}$ and $\beta8^{low}$ GSCs (HBT51), revealing no statistically significant differences in TGFβ1 protein levels. **(C);** VEGF-A ELISA from freshly sorted $\beta8^{high}$ and $\beta8^{low}$ GSCs (HBT51), revealing lack of integrin-dependent differences in VEGF-A protein levels. **(D, E);** Analysis of the Mouse Brain RNA-Seq database reveals that vascular endothelial cells and microglia in the brain are the major sources of tgfbr2 (D) and tgfb1 (E). **(F);** Differential expression of ITGAV, ITGB8 and TGFBR2 mRNAs in various tumor regions based on analysis of the IVY GBM database.

Supplemental Figure 8. FACS-based quantitation of αv integrin and CD133 expression in cultured GBM spheroids. (A-C); Unfractionated tumor cells from three different GBM spheroid cultures were analyzed for αv integrin and CD133 expression. Note that the majority of GBM cells express αv integrin, but only a fraction of those cells also express CD133.

Supplemental Figure 9. RNAi-mediated silencing of ITGB8 in high passage GSCs does not inhibit tumorigenesis in vivo. (A, B); Passaged GBM cells were infected with lentiviruses expressing GFP and non-targeting (NT) shRNAs or shRNAs targeting ITGB8 (A) or ITGAV (B). Immunoblot analysis showing diminished integrin protein expression in cells integrin shRNAs. **(C-H);** Passaged GBM cells were infected with lentiviruses expressing NT shRNAs (C, D) or shRNAs targeting ITGB8 (E, F) or ITGAV (G, H) and injected into the brain. Coronal sections through the brain reveal GFP-expressing tumors (C, E G). H&E staining of fixed sections reveals intracranial tumors in mice injected with all cell types (D, F, H). **(I);** ITGB8 mRNA levels were quantified by RT-PCR in three different high passage GBM spheroids (GSC2, GSC11 and GSC23). Spheroids were grown in serum-free media or were induced to differentiate by serum exposure. Note that differentiation correlates with increased ITGB8 levels in the spheroid samples.

Supplemental Figure 10. Targeting ITGB8 in high passage GSCs using Crispr-Cas9 methods does not block tumorigenesis in vivo. (A); Lysates from passaged GSCs (GSC11) infected with three different lentiviruses expressing GFP, Cas9 and gDNAs targeting ITGB8 were immunoblotted for β8 integrin protein. **(B);** A PCR-based strategy was used to identify Crispr/Cas9-induced mismatch mutations in ITGB8 based on heteroduplex formation. Note that heteroduplexes are detected with both gDNAs that target ITGB8. **(C);** Mismatch mutations

leading to heteroduplexes are not detected in three putative off-target genes, as determined with the Surveyor Mutation Detection Kit. **(D, E);** Primary GBM cells infected with lentiviruses expressing Cas9 or Cas9 and gDNAs targeting ITGB8 were intracranially injected into the striatum of NOD-SCID mice. Note that GBM cells expressing β8 integrin or lacking β8 integrin generate malignant tumors in vivo. H&E-stained brain sections reveal diffuse tumors.

Supplemental Figure 11. β8 integrin regulates cell cycle gene expression in GSCs. (A, B); $\beta8^{high}$ and $\beta8^{low}$ primary tumor cells were fractionated from three different freshly resected primary human GBM samples and analyzed by RNA sequencing. Shown is a heat map listing cell cycle-related genes that are differentially regulated in fractionated GBM cells.

Supplemental Figure 12. Summary of β8 integrin-dependent pathways in fractionated GBM cells based on whole transcriptome sequencing. NES pathway analysis of β8 integrin-dependent pathways that are elevated in $\beta8^{high}$ GBM cells.

Supplemental Figure 13. Analysis of β8 integrin-dependent pathways in fractionated GBM cells. (A-C); Heat maps showing mRNAs upregulated in $\beta8^{high}$ GBM cells in pathways related to mismatch repair (A), homologous recombination (B) and oocyte meiosis (C).

Supplemental Table 1. Summary of tumor initiation in mice intracranially injected with $\beta8^{high}$ and $\beta8^{low}$ GBM cells. Shown are (i) numbers of GBM cells injected per animal, (ii) weeks allowed for tumor initiation and progression in vivo, and (iii) total numbers of mice injected with each cell type that developed tumors.

Supplemental Table 2. Summary of expression signatures for gene sets that are enriched in $\beta 8^{high}$ GBM cells based on KEGG pathway analyses.

Supplemental Table 3. Summary of expression signatures for gene sets that are enriched in $\beta 8^{low}$ GBM cells based on KEGG pathway analyses.

Guerrero et al., Supplemental Figure 1

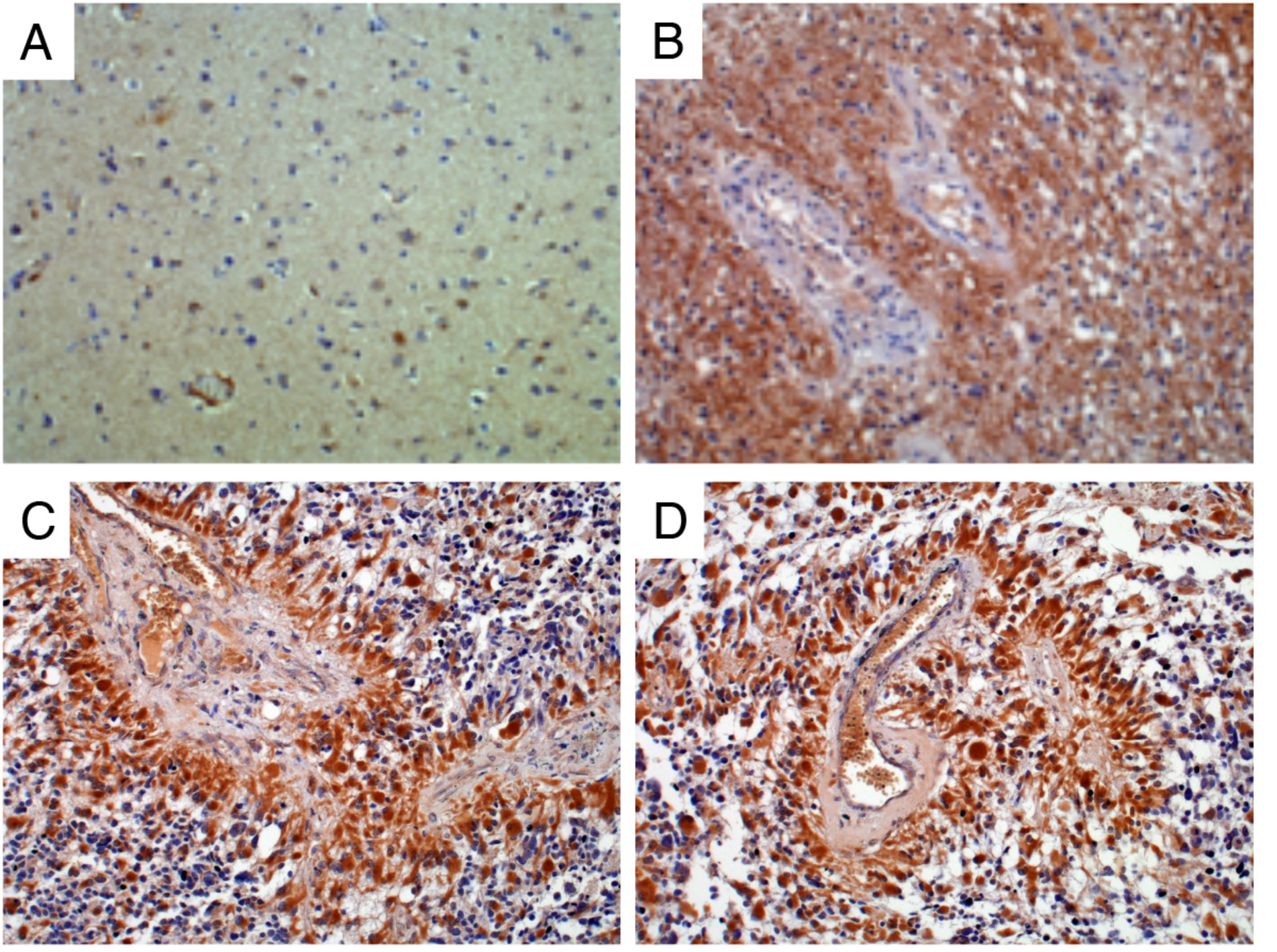

A

Sample	% β8^{high}
9	61
14	13.3
19	0.67
20	0.1
21	2.0
24	19.5
25	6.34
27	0.15
28	22.3
29	0.3
30	71.0
31	0
32	52.6
33	4.3
34	0.5
36	51.2
37	0.3
38	52.6
40	11.3
41	11.8
42	24.4
44	11.0
45	62.9
51	21.1
52	50.1

B

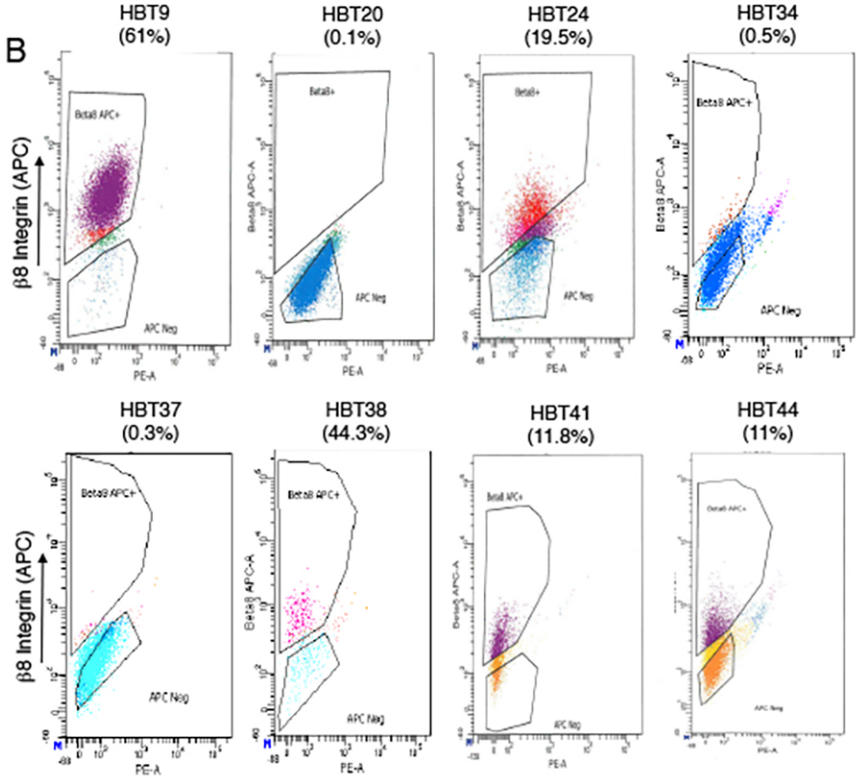

Guerrero et al., Supplemental Figure 3

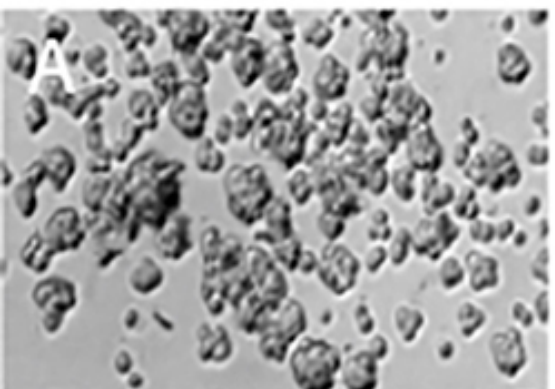

Control IgG

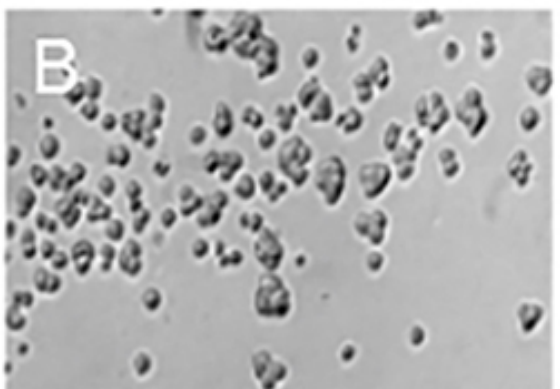

Anti-β8 Integrin

C

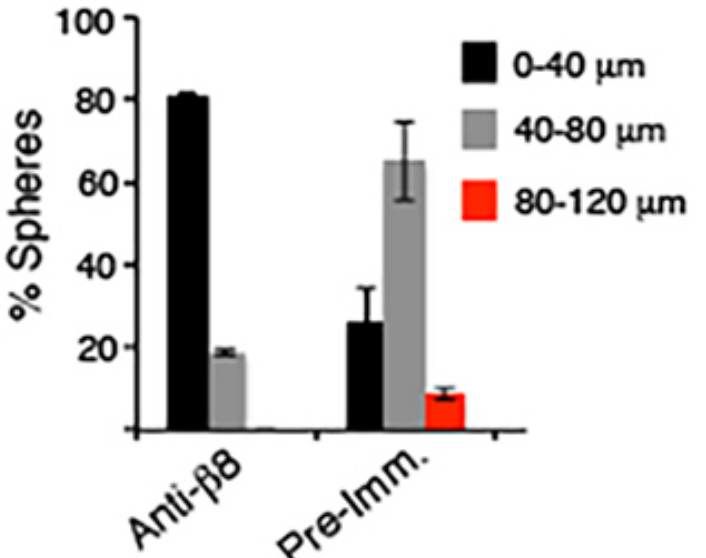

D

MGH26CSC	MGH26FCS	MGH28CSC	MGH28FCS	MGH31CSC	MGH31FCS	
1.794	-6.671	0.893	-3.815	0.185	-0.453	ITGB8 Levels
+++	+	+++	+	+++	+	Tumor

Guerrero et al., Supplemental Figure 4

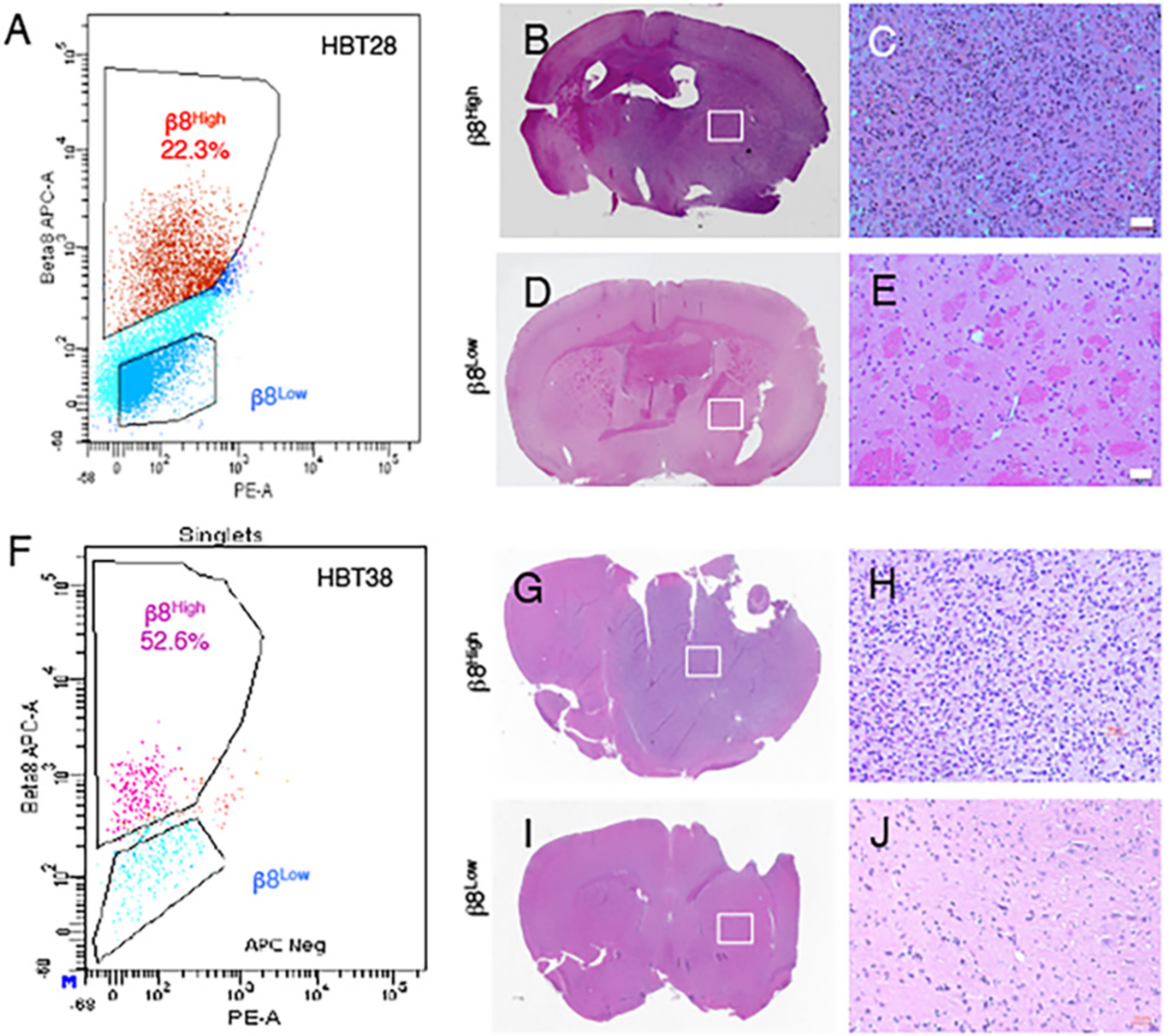

Guerrero et al., Supplemental Figure 5

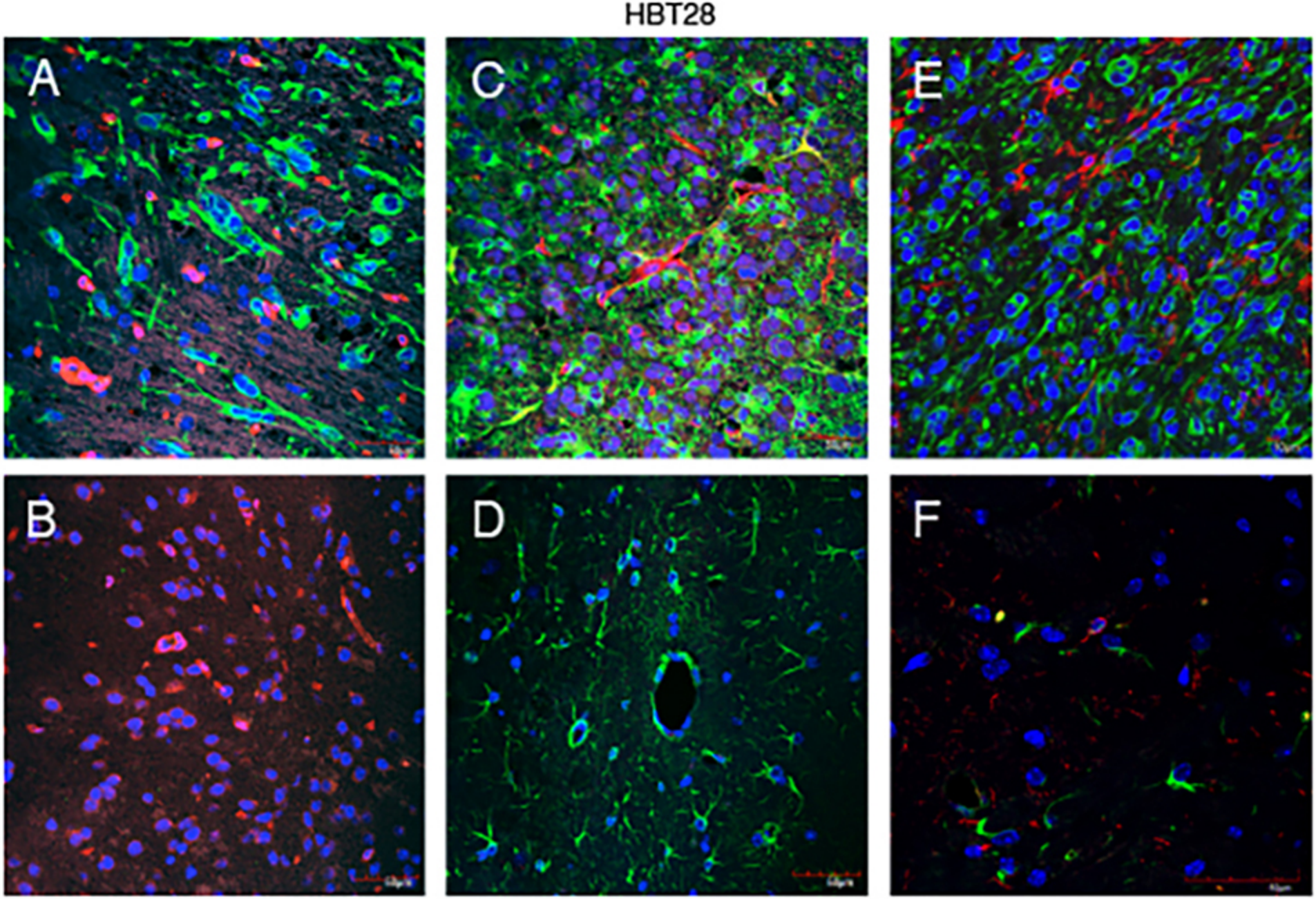

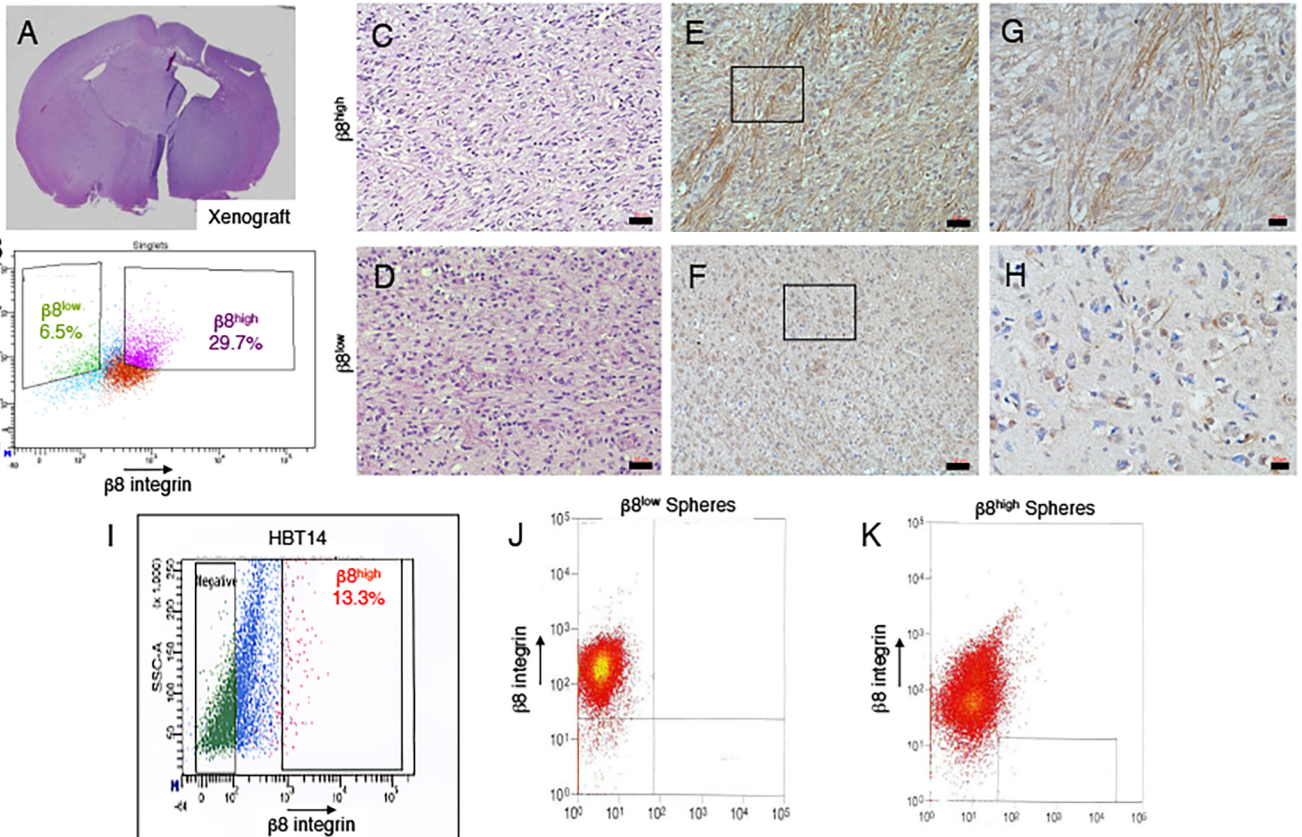
A
Xenograft
B
Singlets
β8low
6.5%
β8high
29.7%
hCD47
β8 integrin
C
D
E
F
G
H
β8high
β8low
I
HBT14
Negative
β8high
13.3%
SSC-A
β8 integrin
J
β8low Spheres
β8 integrin
K
β8high Spheres
β8 integrin

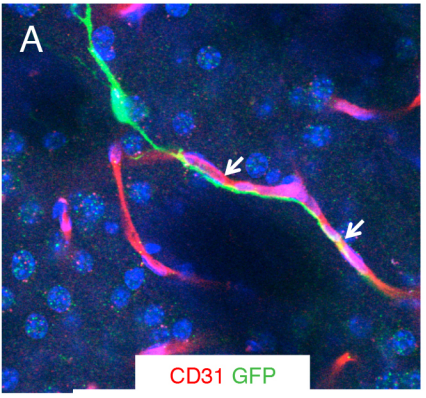
A
CD31 GFP

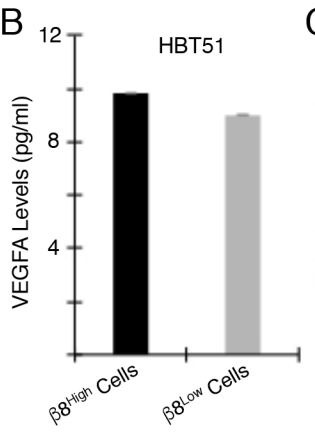
B
HBT51
VEGFA Levels (pg/ml)
12
8
4
β8High Cells
β8Low Cells

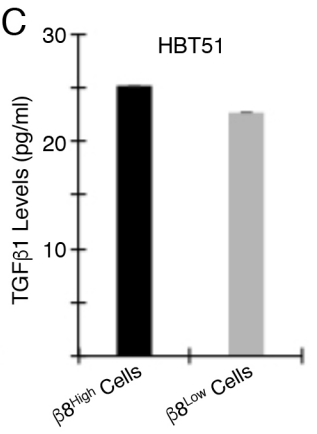
C
HBT51
TGFβ1 Levels (pg/ml)
30
20
10
β8High Cells
β8Low Cells

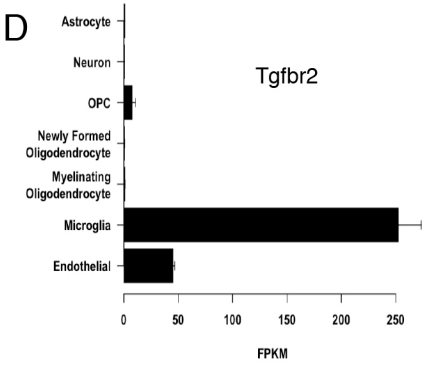
D
Tgfbr2
Astrocyte
Neuron
OPC
Newly Formed Oligodendrocyte
Myelinating Oligodendrocyte
Microglia
Endothelial
0
50
100
150
200
250
FPKM

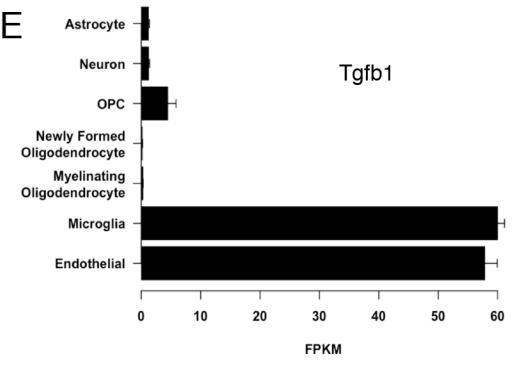
E
Tgfb1
Astrocyte
Neuron
OPC
Newly Formed Oligodendrocyte
Myelinating Oligodendrocyte
Microglia
Endothelial
0
10
20
30
40
50
60
FPKM

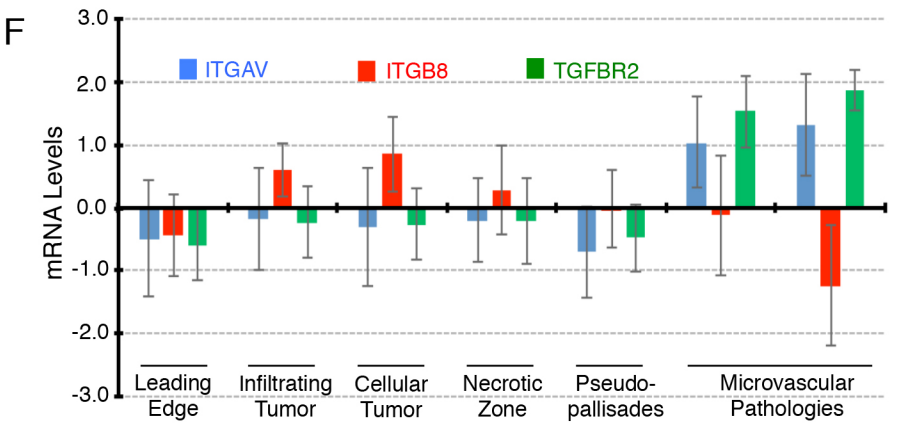
F
ITGAV
ITGB8
TGFBR2
mRNA Levels
3.0
2.0
1.0
0.0
-1.0
-2.0
-3.0
Leading Edge
Infiltrating Tumor
Cellular Tumor
Necrotic Zone
Pseudo-pallisades
Microvascular Pathologies

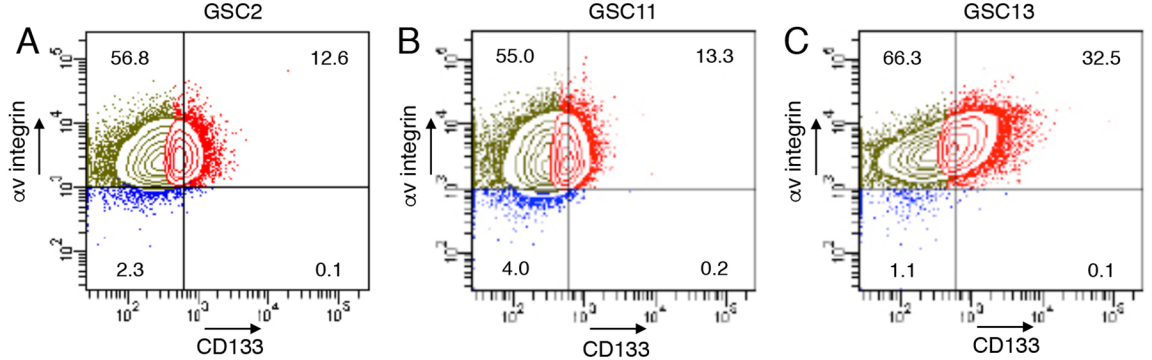
A
GSC2
56.8
12.6
2.3
0.1
αv integrin
CD133
B
GSC11
55.0
13.3
4.0
0.2
αv integrin
CD133
C
GSC13
66.3
32.5
1.1
0.1
αv integrin
CD133

Guerrero et al., Supplemental Figure 9

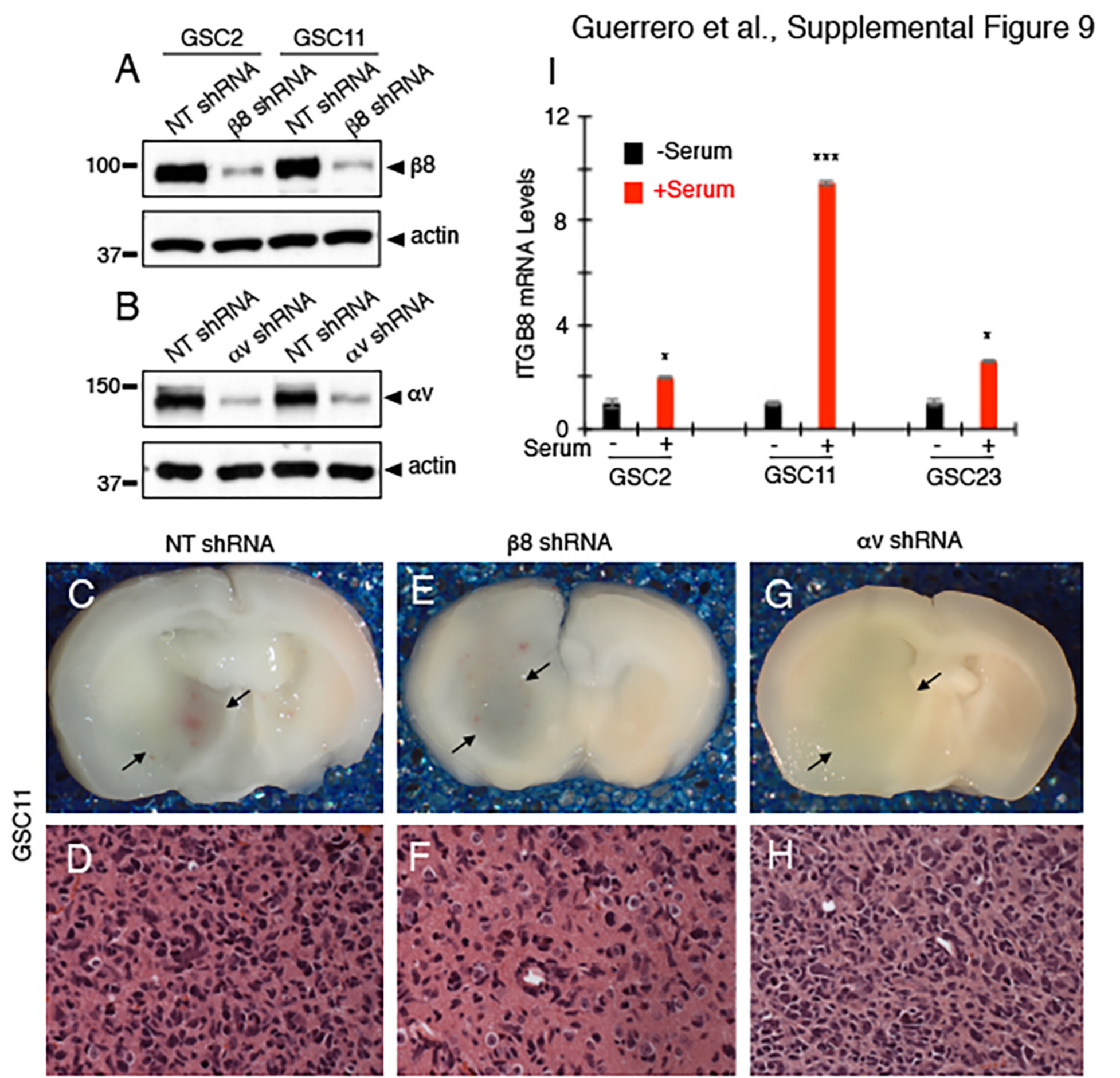

Guerrero et al., Supplemental Figure 10

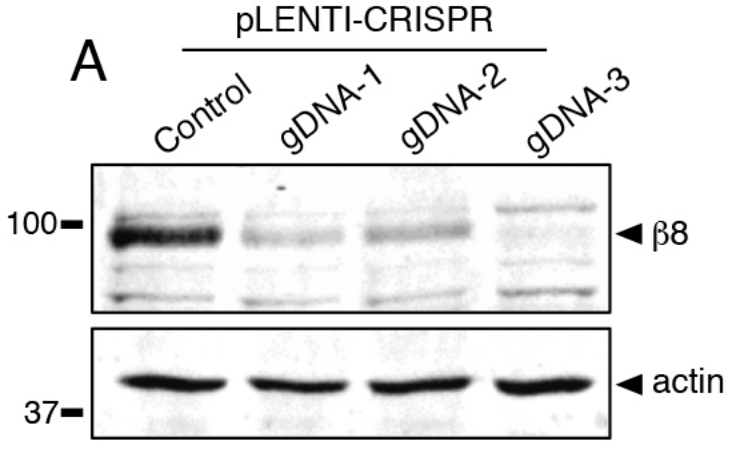

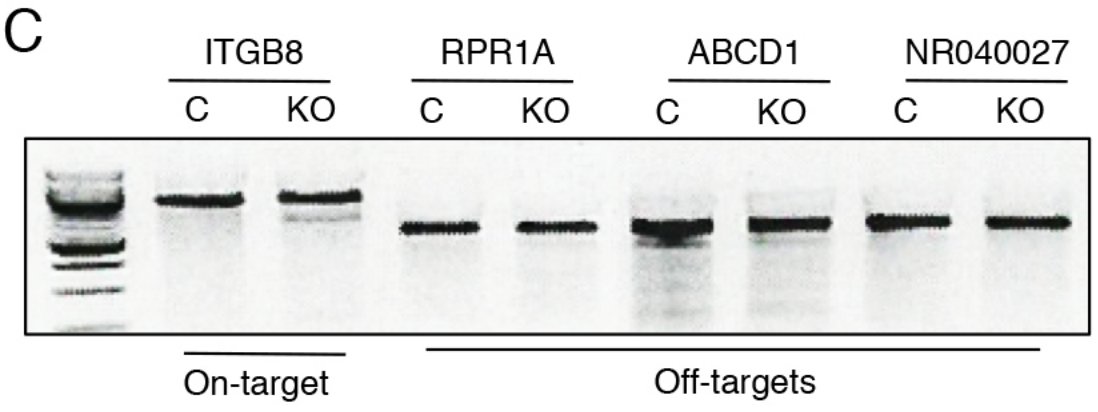

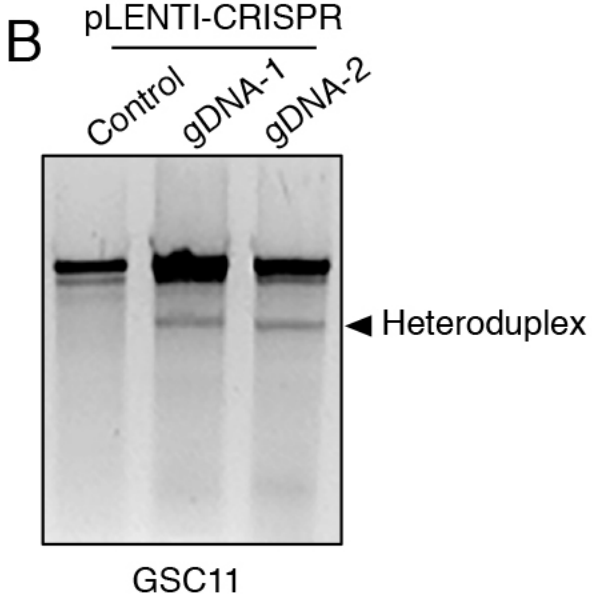

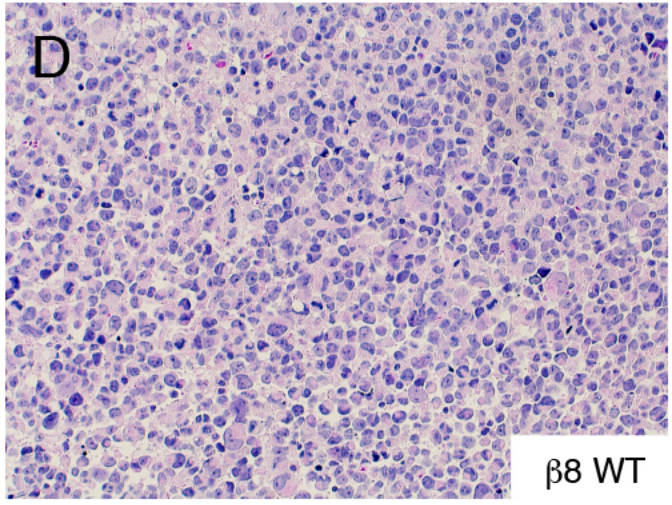

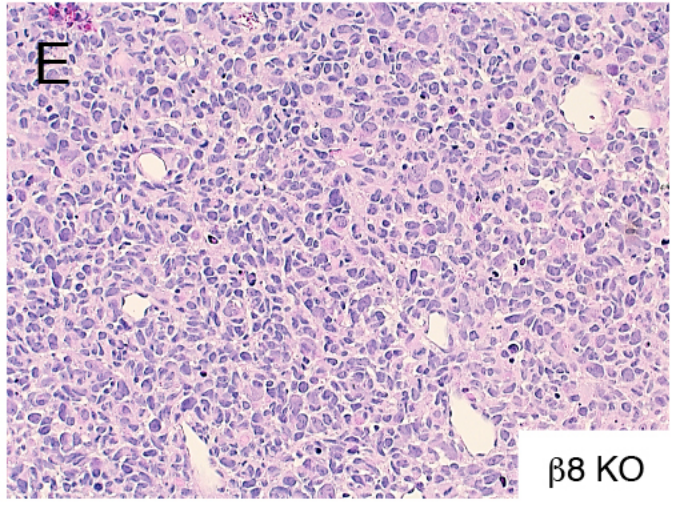

GSC11

Guerrero et al., Supplemental Figure 11

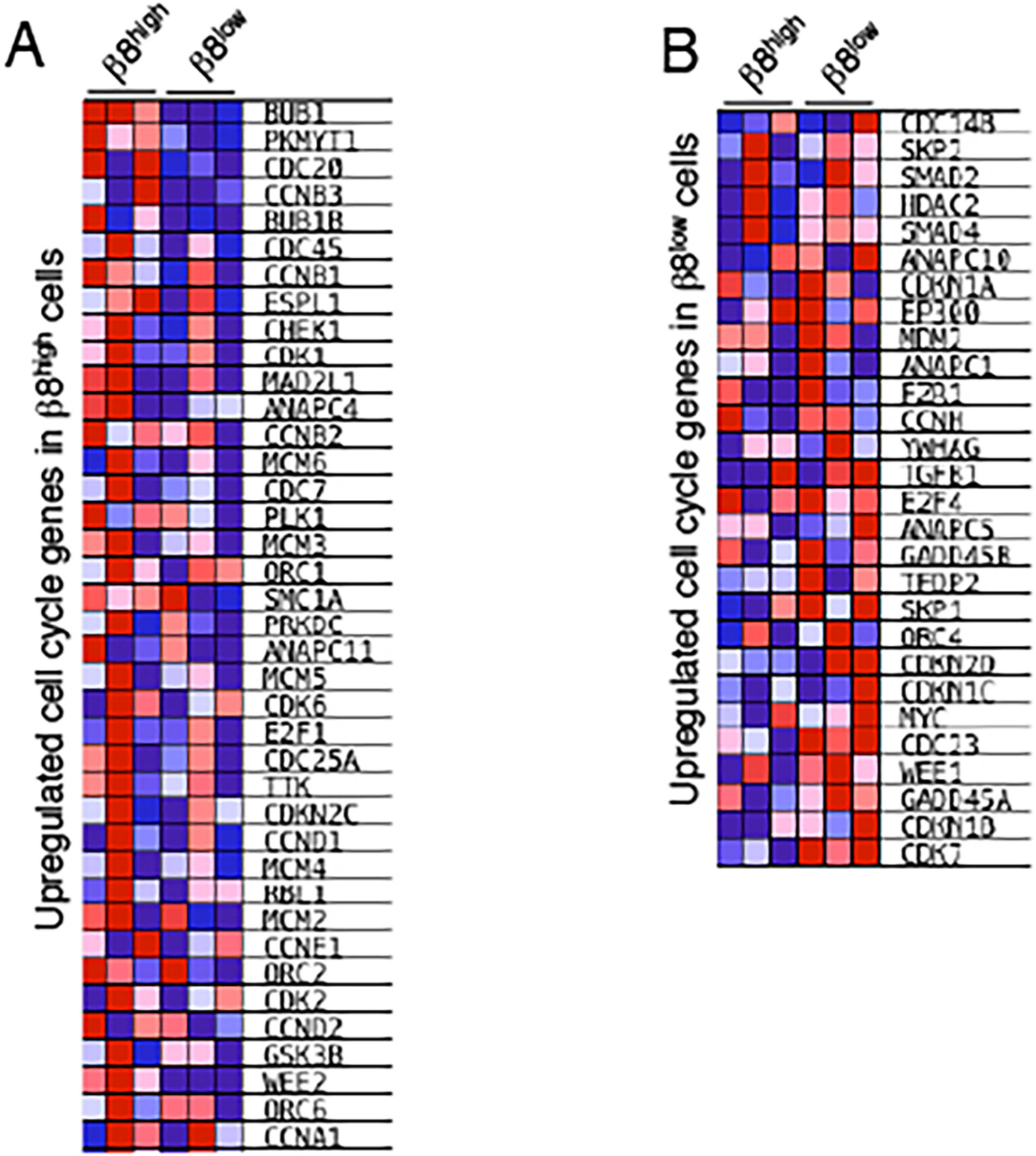

Guerrero et al., Supplemental Figure 12

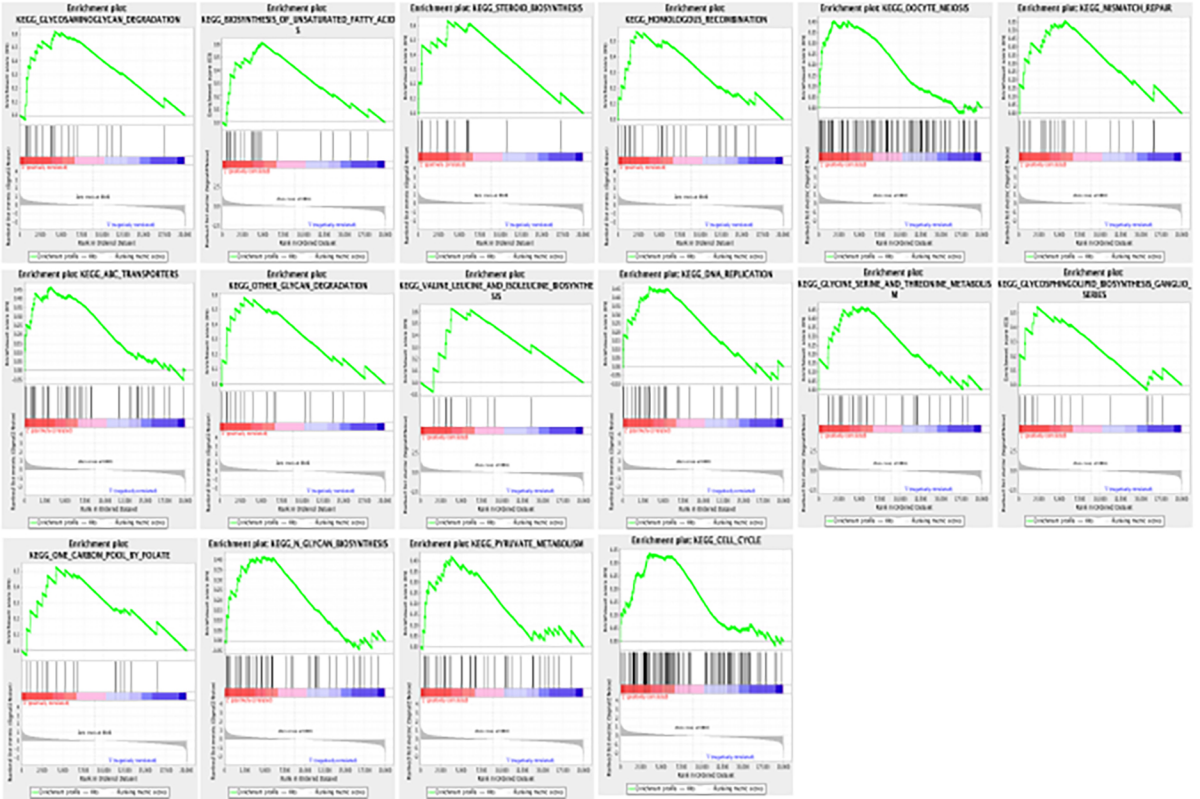

Guerrero et al., Supplemental Figure 13

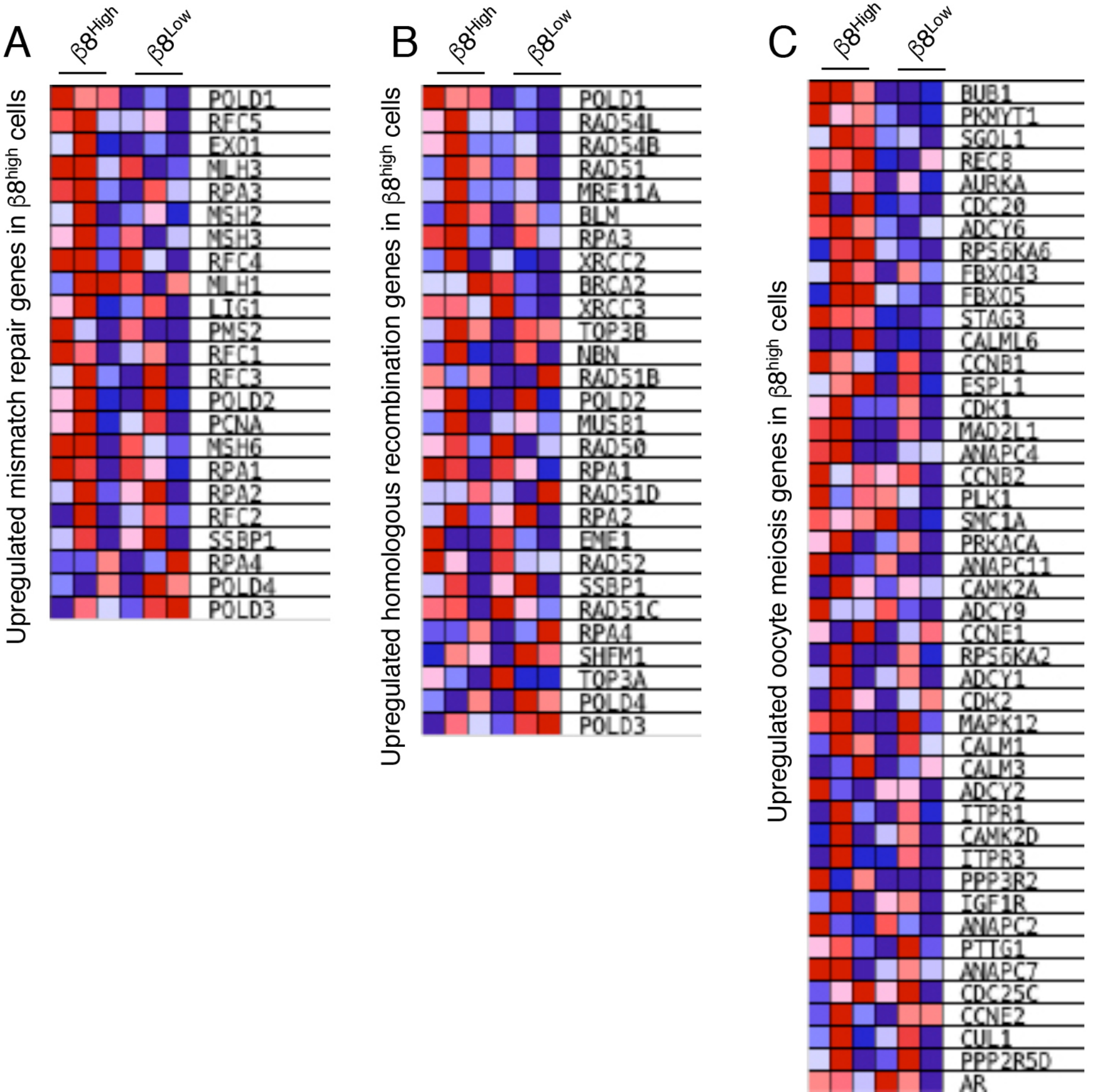

Guerrero et al., Supplemental Table 1

Sample #	# Cells Injected (x 10^3)	Time In Vivo (weeks)	Tumor Incidence	
			$\beta8^{high}$	$\beta8^{low}$
20	200	25	3/3	1/3
21	15	16	3/3	1/2
28	60	18	4/4	0/4
32	100	15	4/4	3/3
34	45	31	1/4	0/4
37	20	24	4/4	2/4
38	12.5	19	4/4	1/4
44	30	18	1/4	0/4
Totals			**24/30 80%**	**8/28 29%**

Guerrero et al., Supplemental Table 2

BIOLOGICAL PROCESS	ES	NES	p-val	FDR q-val
GLYCOSAMINOGLYCAN_DEGRADATION	0.617334	1.8046	0.002315	0.12597813
BIOSYNTHESIS_OF_UNSATURATED_FATTY_ACIDS	0.612531	1.774237	0.004706	0.09057741
STEROID_BIOSYNTHESIS	0.633764	1.73531	0.007143	0.09479308
HOMOLOGOUS_RECOMBINATION	0.56077	1.729852	0.007614	0.07370157
OOCYTE_MEIOSIS	0.404296	1.637817	0	0.13774051
MISMATCH_REPAIR	0.556747	1.627734	0.014286	0.12462507
ABC_TRANSPORTERS	0.46528	1.586172	0.007317	0.15195142
OTHER_GLYCAN_DEGRADATION	0.579413	1.586012	0.035714	0.13337873
VALINE_LEUCINE_AND_ISOLEUCINE_BIOSYNTHESIS	0.627655	1.528212	0.058427	0.18170257
DNA_REPLICATION	0.463349	1.49435	0.023697	0.21051766
GLYCINE_SERINE_AND_THREONINE_METABOLISM	0.465651	1.474975	0.036408	0.2204914
GLYCOSPHINGOLIPID_BIOSYNTHESIS_GANGLIO_SERIES	0.543044	1.463085	0.065315	0.21945165
ONE_CARBON_POOL_BY_FOLATE	0.523933	1.434787	0.06982	0.24705881
N_GLYCAN_BIOSYNTHESIS	0.415028	1.43296	0.036058	0.2333169
PYRUVATE_METABOLISM	0.420752	1.419591	0.040302	0.23732561
CELL_CYCLE	0.338695	1.405206	0.010471	0.2458584

Guerrero et al., Supplemental Table 3

Biological Process	ES	NES	NOM p-val	FDR q-val
RIBOSOME	-0.59058	-2.2274	0	0
LEISHMANIA_INFECTION	-0.59984	-2.1636	0	0
HEMATOPOIETIC_CELL_LINEAGE	-0.55852	-2.05423	0	6.01E-04
GRAFT_VERSUS_HOST_DISEASE	-0.59814	-1.95069	0	0.002462
CYTOKINE_CYTOKINE_RECEPTOR_INTERACTION	-0.43419	-1.87246	0	0.005209
ALLOGRAFT_REJECTION	-0.58428	-1.82833	0	0.008587
SPLICEOSOME	-0.46287	-1.80865	0	0.009783
ASTHMA	-0.6017	-1.78989	0	0.011664
B_CELL_RECEPTOR_SIGNALING_PATHWAY	-0.48902	-1.78491	0	0.010856
PENTOSE_AND_GLUCURONATE_INTERCONVERSIONS	-0.59791	-1.76221	0.005128	0.013619
AUTOIMMUNE_THYROID_DISEASE	-0.5207	-1.7602	0	0.012802
PORPHYRIN_AND_CHLOROPHYLL_METABOLISM	-0.53807	-1.75825	0	0.012188
CHEMOKINE_SIGNALING_PATHWAY	-0.42533	-1.75817	0	0.01125
SNARE_INTERACTIONS_IN_VESICULAR_TRANSPORT	-0.54424	-1.74407	0.001695	0.012114
TYPE_I_DIABETES_MELLITUS	-0.53403	-1.74319	0.001701	0.011429
DRUG_METABOLISM_OTHER_ENZYMES	-0.51725	-1.74015	0	0.010998
CYTOSOLIC_DNA_SENSING_PATHWAY	-0.50249	-1.73369	0	0.011357
BASAL_TRANSCRIPTION_FACTORS	-0.54344	-1.70885	0.005263	0.014423
TOLL_LIKE_RECEPTOR_SIGNALING_PATHWAY	-0.44976	-1.70555	0.001613	0.014033
STEROID_HORMONE_BIOSYNTHESIS	-0.49159	-1.66504	0.00835	0.021253
RNA_POLYMERASE	-0.54982	-1.66416	0.010772	0.020369
FC_GAMMA_R_MEDIATED_PHAGOCYTOSIS	-0.43888	-1.65046	0.001653	0.022273
ASCORBATE_AND_ALDARATE_METABOLISM	-0.56659	-1.64888	0.015929	0.021769
ACUTE_MYELOID_LEUKEMIA	-0.47226	-1.64734	0	0.021357
JAK_STAT_SIGNALING_PATHWAY	-0.40298	-1.62744	0.001555	0.026172
CIRCADIAN_RHYTHM_MAMMAL	-0.6723	-1.61299	0.005181	0.028561
METABOLISM_OF_XENOBIOTICS_BY_CYTOCHROME_P450	-0.44766	-1.59641	0.00495	0.032109
T_CELL_RECEPTOR_SIGNALING_PATHWAY	-0.40768	-1.55512	0.003252	0.04578
INTESTINAL_IMMUNE_NETWORK_FOR_IGA_PRODUCTION	-0.46582	-1.54982	0.012259	0.04617
RNA_DEGRADATION	-0.44053	-1.53839	0.011272	0.049688
NOD_LIKE_RECEPTOR_SIGNALING_PATHWAY	-0.43527	-1.51044	0.010033	0.062338
PROTEASOME	-0.45675	-1.49261	0.031879	0.071017
SYSTEMIC_LUPUS_ERYTHEMATOSUS	-0.38151	-1.49216	0.009188	0.06914
NATURAL_KILLER_CELL_MEDIATED_CYTOTOXICITY	-0.37149	-1.47024	0.007776	0.080483
NITROGEN_METABOLISM	-0.51065	-1.44961	0.057793	0.091849
RIG_I_LIKE_RECEPTOR_SIGNALING_PATHWAY	-0.3981	-1.41841	0.032258	0.11383
PRION_DISEASES	-0.45442	-1.41137	0.053601	0.117182
REGULATION_OF_AUTOPHAGY	-0.44886	-1.395	0.07438	0.1286
THYROID_CANCER	-0.45375	-1.38163	0.062395	0.137798
MAPK_SIGNALING_PATHWAY	-0.32236	-1.37936	0.007052	0.136661
ENDOCYTOSIS	-0.33608	-1.37905	0.02	0.133633
ADIPOCYTOKINE_SIGNALING_PATHWAY	-0.37923	-1.35193	0.05802	0.158664
CHRONIC_MYELOID_LEUKEMIA	-0.3669	-1.32842	0.059801	0.182814
PRIMARY_IMMUNODEFICIENCY	-0.41951	-1.31538	0.104235	0.195698
APOPTOSIS	-0.35327	-1.31332	0.063518	0.193618